Contents lists available at ScienceDirect

Coastal Engineering

journal homepage: www.elsevier.com

Annual prediction of shoreline erosion and subsequent recovery

Mark A. Davidson[a, *], Ian L. Turner[b], Kristen D. Splinter[b], Mitchel D. Harley[b]

[a] Coastal Processes Research Group, Plymouth University, UK
[b] Water Research Laboratory, School of Civil and Environmental Engineering, UNSW, Sydney, Australia

ARTICLE INFO

Article history:
Received 17 January 2017
Received in revised form 31 July 2017
Accepted 15 September 2017
Available online xxx

ABSTRACT

Prediction of the potential impact of an extreme storm-sequence on coastal resilience and the subsequent rate of post-storm recovery is a fundamental goal for coastal scientists, engineers and managers alike. This paper presents a methodology for forecasting shoreline change over annual time-scales, including the prediction of the potential impact of storm sequences and the subsequent post-storm recovery. The methodology utilises an archive of measured or modelled wave data to produce multiple ($\approx 10^3$) synthetic hydrodynamic forcing time-series to drive an equilibrium shoreline model in a Monte Carlo simulation. A Generalised Extreme Value (GEV) analysis is conducted on the resulting shoreline predictions in order to extrapolate the magnitude of shoreline displacements for predefined return periods. Three shoreline displacement bands are defined in a 'traffic light' system, to aid the interpretation of results; a green (normal) band characterising shoreline displacements expected within the typical decade, an amber (high) band defining *events* with return periods outside the decadal recurrence threshold but within return periods <100 years, and a red (extreme) band designed to encompass the theoretical limit of the shoreline predictions. The methodology was tested on two field sites with distinctly contrasting wave climates and tidal regime. The first was Perranporth in the UK with a strong seasonal variability in both the wave climate and shoreline response. The second was Narrabeen, Australia, with a much smaller seasonal variability and more storm-dominated wave climate and shoreline response. In both cases an equilibrium shoreline model (ShoreFor) was calibrated using measured shoreline data and complementary wave data. The prediction methodology was found to be mildly sensitive to the temporal range of the wave data used, with at least 25-years of data required to achieve consistent classification of the magnitude of storm erosion and recovery. Two extreme storm sequences were targeted to test the methodology, the Pasha Bulker storm sequence recorded at Narrabeen in June 2007 and the extreme storm sequence which impacted the UK during the winter period of 2013/14. All wave and shoreline time-series recorded in this period were left unseen in model calibrations and subsequent predictions, in order to provide a rigorous test of the methodology. In all cases the methodology was able to predict both storm erosion and subsequent recovery and give a clear indication of the intensity of the shoreline displacement. The storm sequences studied forced shoreline displacements rated as high at Narrabeen and extreme at Perranporth and both sites displayed rapid post-storm recovery. The impact of extreme storms on shoreline recession and subsequent post storm recovery is predictable at these energetic cross-shore transport dominated sites, promising the potential for a new coastal management tool.

1. Introduction

Arguably the 'holy grail' for coastal scientists and engineers is to derive sufficient knowledge and understanding of coastal systems to be able to forecast coastal erosion and accretion with a level of confidence and lead time to permit effective coastal management decisions to be made regarding the use, development and protection of coastal environments. Important coastal management questions addressed here are: What are the potential storm impacts on the coastline? Will the coast recover from the prior violent storm(s) and how long will this recovery take?

Recent developments in process based morphodynamic models and computer speed mean that long-term simulations of coastal evolution are now feasible (Walstra et al., 2012, 2016; Callaghan et al., 2013). Intuitively, one might expect that the more sophisticated the morphodynamic model, the more accurate and robust the coastal evolution predictions might be, even with the trade-off of significant computational time. However, this will only be the case if the extra model sophistication carries with it increased predictive skill over simpler modelling approaches, which is often not the case for long-term predictions of the order of a year or more.

Common coastal state indicators used by managers to assess the current health of the coastline and resilience to coastal erosion and flooding frequently include some measure of beach volume or shoreline position (Davidson et al., 2007; Kroon et al., 2007). In this contribution, a 'simpler' methodology appropriate to forecasting these

* Corresponding author.
Email address: mdavidson@plymouth.ac.uk (M.A. Davidson)

https://doi.org/10.1016/j.coastaleng.2017.09.008
0378-3839/

indices is investigated, rather than the complex time-varying and 3-dimensional structure of the beach surface. Although shoreline prediction is the focus of this study, intertidal beach volumes have been shown to be coherent with shoreline evolution (Farris and List, 2007; Harley et al., 2011; Robinet et al., 2016) and therefore the approach developed here is expected to be transferable.

Recently, models of 'reduced complexity' (Farris and List, 2007; Murray, 2007, French et al., 2016) have been shown to provide skilful hindcasts of coastal change on both cross-shore (Davidson and Turner, 2009; Davidson et al., 2010; Yates et al., 2009, 2011; Splinter et al., 2014; Larson and Kraus, 1989; Callaghan et al., 2008) and longshore transport dominated (Hanson and Kraus, 1989; Hanson, 1989; Turki et al., 2013; Ashton et al., 2001; Ashton and Murray, 2006) coastlines. The simplicity and stability of such models unlocks the exciting potential for much longer-term (months-years-decades) hindcasts and even forecasts of coastal change.

Skilful hindcasting of coastal evolution with known forcing conditions is a necessary precursor to forecasting of future coastal change. Short-term deterministic forecasts with a 5- to 10-day prediction horizon can be achieved with the aid of accurate forecasts of wave forcing derived from physics-based weather models (Baart et al., 2016). However, at prediction horizons in excess of this one must fall back on climatological/statistical approaches to forecasting. The latter approach is the subject of the present paper, which develops predictions up to (and potentially beyond) one year. Climatological approaches can be particularly skilful in predicting weather, when there is a strong, coherent seasonal variability, for example, annual fluctuations in air temperature or wind speed. Although there are some examples of climatological shoreline forecasting (e.g (Callaghan et al., 2008, 2013; Baart et al., 2016).), this research area is still in its infancy.

In this contribution we use a methodology similar to the Extended Streamflow Prediction (ESP) used historically in hydrology for predicting river discharge from historic rainfall data. In ESP historic rainfall records are used to force hydrological models for river discharge. The output of the models is then analysed statistically to evaluate normal and extreme discharge return levels (Day, 1985). This is in contrast to other methods of predicting extremes which first perturb the forcing and then take the model output at face value (Day, 1985; Cloke and Pappenberger, 2009). The ESP analysis by contrast, takes the historic forcing data and assumes that each year of past meteorological data is a possible representation of the future and requires extrapolation of the model output to derive estimates of future extremes.

In this paper multiple synthetic wave time series are derived from a pool of measured data and subsequently used to force multiple shoreline simulations using a simple equilibrium model. Monte Carlo methods have been implemented for the prediction of shoreline change in the past (e.g (Davidson et al., 2010; Ruggiero et al., 2006; Reeve et al., 2014).), however the approach taken here is somewhat different. A robust statistical generalised extreme value (GEV) analysis is used on the shoreline predictions to extrapolate the magnitude of shoreline displacement for pre-defined return periods. Details of the two field sites with contrasting wave climates and tidal regimes, which are used to test the forecasting methodology is given is Section 2. This is followed by an overview of the forecasting methodology in Section 3, including a description of the shoreline model, the method of generating multiple synthetic wave records using measured or modelled data and finally the method of generalised extreme value analysis (GEV), which gives shoreline displacements for specified return periods. In Section 4 the results of this procedure are presented for both the storm and recovery period of two major storms experienced at two contrasting sites. The finding of this research and future developments are summarised in Sections 5.

2. Site description

Two extensive shoreline datasets and complementary wave measurements at highly contrasting environments (Table 1) are used to provide a rigorous test of a shoreline prediction methodology. Both environments are energetic, cross-shore transport dominated, swash-aligned coastlines, but each has very different temporal variability in their wave climate and shoreline response. Specifically, the two sites are: Perranporth, with a highly seasonal wave climate, located on the exposed Atlantic west coast of Cornwall in the UK (Davidson et al., 1997) and Narrabeen, with a storm dominated wave climate, located on Sydney's northern beaches on the eastern seaboard of Australia (Turner et al., 2016), (Fig. 1). A summary plot showing the seasonal succession of ensemble-averaged parameters that will be subsequently used to force the shoreline model and the measured shoreline responses for both Perranporth and Narrabeen are shown in Fig. 2. The forcing parameters include wave power and dimensionless fall velocity, $\Omega = H_b/\omega T$ (Gourlay, 1968), where H_b is the breaker height, ω is the fall velocity of the beach sediment and T is the peak wave period. Here H_b is computed from the offshore significant wave height and period (Splinter et al., 2014).

The Perranporth wave data in Fig. 2 is based on a 65-year record of hourly Wave Watch III modelled offshore (73 m depth) significant wave height and period data for the location of the Sevenstones Lightship (Dodet et al., 2010) and a complementary time-series of the cross-shore position of the shoreline, extracted from GPS surveys conducted over an 8-year period (Masselink et al., 2014a). The Narrabeen data used here includes a 36-year record of hourly offshore wave statistics, measured at Sydney's wave rider buoy (depth 74 m) and a complementary 8-year time-series of shoreline displacements. For consistency, shorelines at both sites were centred on the mean high-water contour line, which was averaged over a 400 m longshore distance and sampled at monthly time intervals.

2.1. Perranporth, UK

Perranporth, is a 3.5 km long, macrotidal (mean spring tidal range 6.5 m) beach situated on the northern coast of the UK's southwest peninsula (Fig. 1a). It is directly exposed to normally incident, energetic and highly seasonal swell waves generated by anticyclones propagating on a general westerly track across the northern Atlantic Ocean. This seasonality in the wave climate is shown clearly in the

Table 1
Comparative data/site characteristics for Perranporth and Narrabeen, including annual average deep-water wave characteristics and sediment properties. $\sigma_{\Omega 360}/\sigma_{\Omega 30}$ is a seasonality index (Splinter et al. (2014).,) describing the ratio of the average annual to monthly standard deviation in dimensionless fall velocity, higher values indicating increased seasonality. Notice that seasonality at Perranporth is some 20% higher than Narrabeen and that dimensionless fall velocities are double a Perranporth indicating more dissipative beach states.

Site	Hs [m]	Tp [m]	Ω	D50 [mm]	ω [m/s]	$\sigma_{\Omega 360}/\sigma_{\Omega 30}$	Survey Method(interval)	Wave data[Yrs]	Wave Measurement(type)	Depth
Perranporth	1.98	8.3	5.30	0.33	0.04	1.22	Survey(monthly)	63	Sevenstones(modelled)	73
Narrabeen	1.62	9.6	3.67	0.40	0.05	1.07	Video(weekly)	36	Sydney(measured)	74

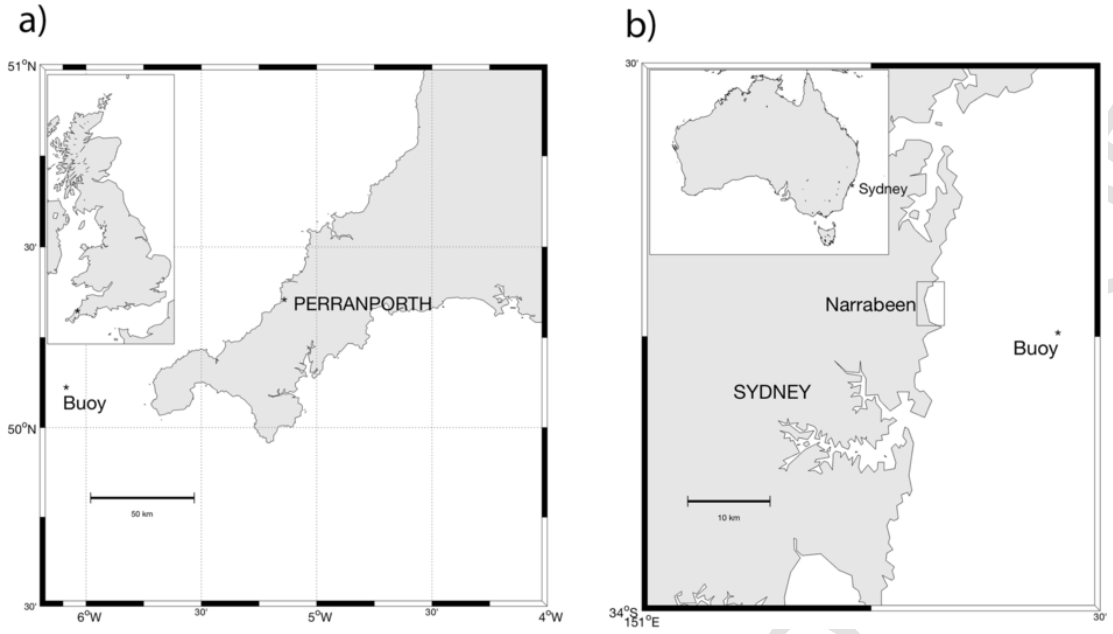

Fig. 1. Location map for a) Perranporth, Cornwall, UK and b) Narrabeen, NSW, Australia.

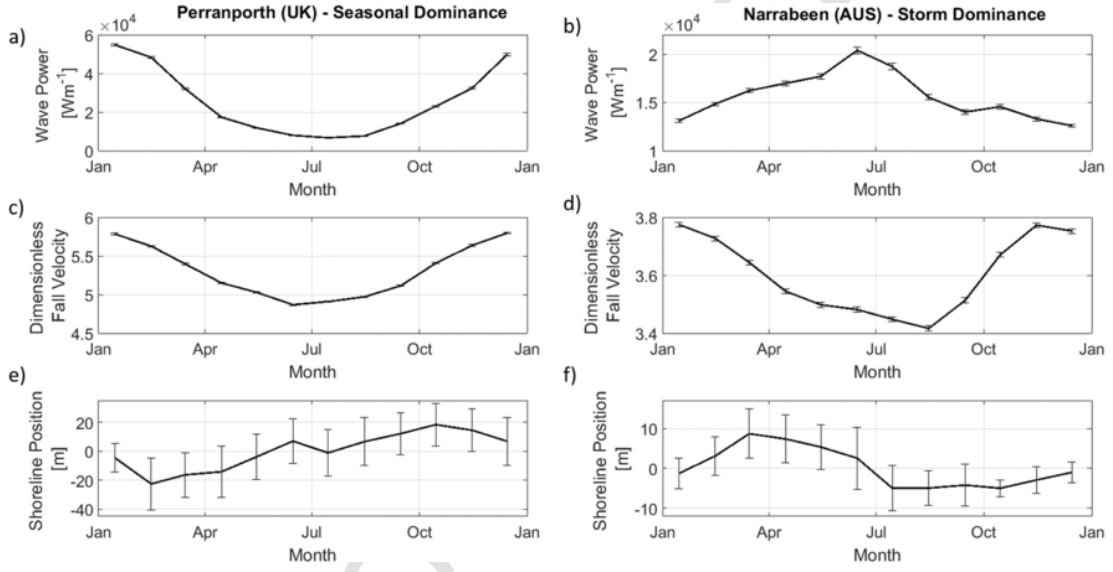

Fig. 2. Monthly ensemble averages offshore wave power (top), dimensionless fall velocity (middle) and shoreline displacement (bottom) for Perranporth, UK (left) and Narrabeen, Australia (right). Ensemble means are presented with 95% confidence interval bars in all cases. The number of years of wave data in the ensembles for Perranporth and Narrabeen are 63 and 36 years respectively. For both sites over 8-years of shoreline data have been ensemble averaged.

monthly-averaged wave power, where energetic, long-period swell waves arriving during the November to January are ≈5.5 times higher than the (June–August) summer months (Fig. 2a).

Beach sediments are comprised of quartz sand with average D_{50} of 0.33 mm and a fall velocity of 0.04 m/s (Prodger et al., 2015). Monthly-averaged dimensionless fall velocities at Perranporth are in the range (4.5–6) indicating intermediate to dissipative beach states which are consistent with observations. The modal classification at Perranporth is low-tide bar and rip according to the classification of Masselink and Short (1993). However, winter periods are often typified by highly dissipative beach states.

The shoreline response at Perranporth (Fig. 2e) shows high variance at annual time-scales, with shoreline erosion commonly evolving smoothly over the November to February fraction of the year in response to a succession of erosive storms, rather sharp step-like displacements relating to individual storm events (Fig. 2). During this winter storm season the horizontal displacement of the mean high water contour can be very large, exceeding 70 m. Beach recovery begins in late March and proceeds at a much slower rate (≈ 1/4) than the erosion, often persisting until October.

Interannual variability in the wave climate is dominated by the North Atlantic Oscillation Index with more positive values being indicative of stronger westerly winds and waves (Masselink et al., 2014a), although the direct link with shoreline erosion and morphology remains unsubstantiated (Thomas et al., 2012).

2.2. Narrabeen, Australia

Narrabeen is a microtidal (mean spring tidal range ≈ 1.5 m), 3.5 km long, embayment, situated on Sydney's northern beaches (Fig. 1b). The Narrabeen wave climate is dominated by two principle components. The first is a moderate to high energy condition which prevails from the S/SE with a mean period and wave height of $T_p \approx 10$ s and $H_s \approx 1.6$ m respectively and is generated by mid-latitude cyclones propagating over the Tasman Sea (Short and Trenaman, 1992; Harley et al., 2010). The second component are storm events ($Hs > 3$ m) which represent 6% of the observed wave field (Lord and Kulmar, 2000). Storms vary seasonally, with most storms occurring in winter (39%), fewest storms occurring in summer (12%) and transitional periods observed in autumn (26%) and spring (23%) (Harley et al., 2010). Winter storms are characterised by high power waves from a S/SE direction generated by mid-latitude cyclones from the south and east coast low pressure systems. Notice however that the maximum monthly-averaged offshore wave power at Narrabeen is only a third of that observed at Perranporth (Fig. 2b and c). The summer wave climate is dominated by NE short period waves generated by a local sea breeze (Short and Trenaman, 1992). Interannual variability in the Sydney wave climate is influenced by the Southern Oscillation Index, in particular the La Niña phase is associated with an increase in storm frequency and duration with a dominant NE/E direction, whereas El Niño phase is characterised by milder SE/S wave conditions (Harley et al., 2010; Ranasinghe et al., 2004).

Narrabeen is characterised by coarser sand ($D_{50} \approx 0.4$ mm) than Perranporth and monthly-mean dimensionless fall velocities ($\Omega = 3.4–3.8$) that are indicative of the range of intermediate beach states that are observed, including both welded and detached bar states. Interestingly, dimensionless fall velocities are lowest in the Austral winter even though winter waves are more energetic. This factor relates to the longer wave periods associated with the winter swell.

The surfzone width at Narrabeen is relatively narrow compared to Perranporth, leading to efficient sediment transport between the beach face and sandbars and more rapid shoreline displacements, which typically proceed at monthly (storm) time-scales. In spite of this rapid shoreline response there is also a significant seasonal signal at Narrabeen, with erosion during the months of April to July and beach recovery predominantly in the subsequent November to March period (Fig. 2f). Maximum shoreline displacements at Narrabeen are half (≈ ±20 m) that observed at Perranporth and the seasonal range less than a quarter (≈ ±10 m, Fig. 2e and f). Splinter et al. (2014)., characterised the relative seasonal to storm dominance by the ratio of the yearly- and monthly-average standard deviations in dimensional fall-velocity ($\sigma_{\Omega 365}/\sigma_{\Omega 30}$), whereby values significantly greater than 1.0 typify highly seasonality. The storm dominance at Narrabeen is again highlighted by the observed value of $\sigma_{\Omega 365}/\sigma_{\Omega 30} = 1.07$, which is some 13% lower than that observed at Perranporth (1.22). Due to this storm dominance it might be expected that the shoreline dynamics of this Pacific east coast site will be the most challenging to predict meaningful shoreline responses due to the episodic nature of the storms.

2.3. Extreme storms

In this section, we focus on two notable extreme storm sequences recorded at Perranporth and Narrabeen. At Perranporth the extreme storms in the November–February period of 2013/14 produced the most powerful sequence of waves observed in the past 65-years causing over 70 m of shoreline recession. Masselink et al. (2014b)., reported that 22 storms (each >1% exceedance in offshore significant wave height) were observed in this period. At Narrabeen the model will be tested on a powerful sequence of extreme storms recorded during the La Niña year in June 2007, which caused the bulk tanker Pasha Bulker to run aground on a beach north of the site and resulted in over 35 m of shoreline recession at Narrabeen (Harley et al., 2016), hereafter referred to as the 'Pasha Bulker storm'. This storm sequence was third largest in terms of beach erosion volumes above mean sea level 73 m^3/m) recorded at Narrabeen in the past 40 years, with the second and third largest storms eroding 76 m^3/m (May 1997) and 103 m^3/m (June 2016) respectively.

3. Prediction methodology

This section briefly describes the equilibrium shoreline model that is used to derive the shoreline predictions. A detailed description of the model is avoided here and instead the Reader is directed to Davidson et al. (2013)., and Splinter et al. (2014)., for a more thorough description and validation of the model. After the brief description of the model, details of the calibration and validation are given. This is followed by a description of the simulation of the synthetic wave forcing parameters that are used to force the shoreline model in a Monte Carlo fashion and form the basis of the generalised extreme value analysis.

3.1. ShoreFore - model description

The shoreline change with time is expressed as a function of the incident wave power (P) and the disequilibrium in the dimensionless fall velocity $\Delta\Omega$.

$$\frac{dx}{dt} = c^{\pm} P^{0.5} \Delta\Omega \tag{1}$$

Here c is the response rate coefficient that controls the magnitude of the shoreline response per measure of wave power [$m/(W/m)^{0.5}$]. The response rate parameter takes different values depending on whether the shoreline is eroding or accreting. The sign of the shoreline displacement is controlled by the disequilibrium in the dimensionless fall velocity ($\Delta\Omega$), which is given by:

$$\Delta\Omega = \frac{1}{\sigma}\left(\Omega_{\phi} - \Omega\right) \tag{2}$$

Here Ω is the instantaneous dimensionless fall velocity and Ω_{ϕ} is a weighted average of the antecedent dimensionless fall velocity by the following weighting function (Wright et al., 1985):

$$\Omega_{\phi} = \left[\sum_{i=0}^{2\phi} 10^{-i/\phi}\right]^{-1} \sum_{i=0}^{2\phi} \Omega_i 10^{-i/\phi} \tag{3}$$

and σ is the standard deviation of (Ω_{ϕ}-Ω), such that $\Delta\Omega$ has unit standard deviation and primarily controls the sign of the shoreline change. The model predicts erosion when incident waves are steeper than the weighted average (antecedent) conditions and visa-versa for accretion. A strong hysteresis in the shoreline behaviour is implicit in this model, whereby future change is highly dependent on the antecedent forcing conditions. Thus, predictions of shoreline position are not just a function of the future forcing conditions, they are also

strongly influenced by the antecedent conditions. The parameter ϕ is measured in days and controls the decay in the weighting function which has a value of one at the prediction time, decaying to 0.1 and 0.01 at ϕ and 2ϕ days respectively before the prediction time. The value of ϕ effectively controls the frequency of the shoreline response with values $>>10^2$ days producing a dominantly seasonal shoreline response (given some seasonality in the observed wave climate), typical of dissipative beaches, whilst values $<10^2$ days produce a higher frequency storm response, typical of more intermediate beaches (Splinter et al., 2014). Note that for a given site with consistent grainsize, the variability in the forcing parameters (P and Ω) is controlled only by hydrodynamic variables (H_b and T). We require synthetic values of these parameters, which reflect the observed seasonal statistics of the wave field, in order to generate the shoreline predictions.

3.2. Model calibration

Fig. 3 shows the wave power time-series alongside the respective model calibrations and validations for both the Perranporth and Narrabeen data sets. Here the two major storm sequences have been omitted from the model calibration and have been used here to validate the models capacity to hindcast two major storm events, using measured forcing parameters. These storms are the Pasha Bulker storm sequence in June 2007 at Narrabeen and the extraordinary storm sequence which struck the exposed energetic coastlines of the north Atlantic during the winter of 2013/14. These storms will be used later to test the prediction method and the true wave forcing for these periods will remain unseen for both the model calibration and the later predictions in order to provide a rigorous test of the methodology.

As shown in Fig. 3, model hindcasts are highly skilful at matching observations for both calibration ($r = 0.92$ Perranporth; $r = 0.87$ Narrabeen) and validation ($r = 0.98$ - Perranporth; $r = 0.89$ - Narrabeen) subsets of the data at both sites. It is noted that the model optimised ϕ values for both sites are 15 days for Narrabeen, typical values for a storm-dominated intermediate beach, in contrast to 450 days for Perranporth, in keeping with this contrasting site exhibiting a seasonally-dominated dissipative beach.

3.3. Generating synthetic time-series

A quasi-Monte Carlo simulation method is adopted here for predicting the shoreline climatology. A similar method of shoreline forecasting was suggested by Davidson et al. (2010), who implemented the method of Borgman and Scheffner (Borgman and Scheffner (1991) to generate synthetic wave series based on the monthly, statistical variability in wave height, period and direction in the measured wave field. This contribution moves on from this work by implementing a different method of synthetic wave generation, and the application of a more sophisticated GEV analysis of the model output.

Generation of synthetic waves involves the assembly of a large number of forcing time-series, used later to drive the shoreline model. The key forcing parameters for the ShoreFor model are wave power (P) and dimensionless fall velocity (Ω) time-series. These synthetic series must reflect the measured or modelled statistical properties for the prediction site. Each of the resulting forcing series are used to generate a shoreline prediction using the calibrated ShoreFor model detailed in the previous section. Typically, $N = 10^3$ synthetic time-series are generated for the Monte Carlo simulations. The sensitivity of the forecasting method to number of synthetic series is investigated later in this paper. A rigorous statistical GEV analysis of the resulting shoreline data is then used to extrapolate the magnitude of both shoreline accretion and erosion at specified return periods.

In the present contribution, we restrict our prediction horizon to one year. This is done because a meaningful multiyear prediction requires additional knowledge of the likely inter-annual variability. The prediction methodology used here does not include this, although work is currently in progress to extend the predictions in this direction.

A pool of either modelled (i.e. Perranporth), measured or a combination of these (i.e. Narrabeen) wave data is used to generate new

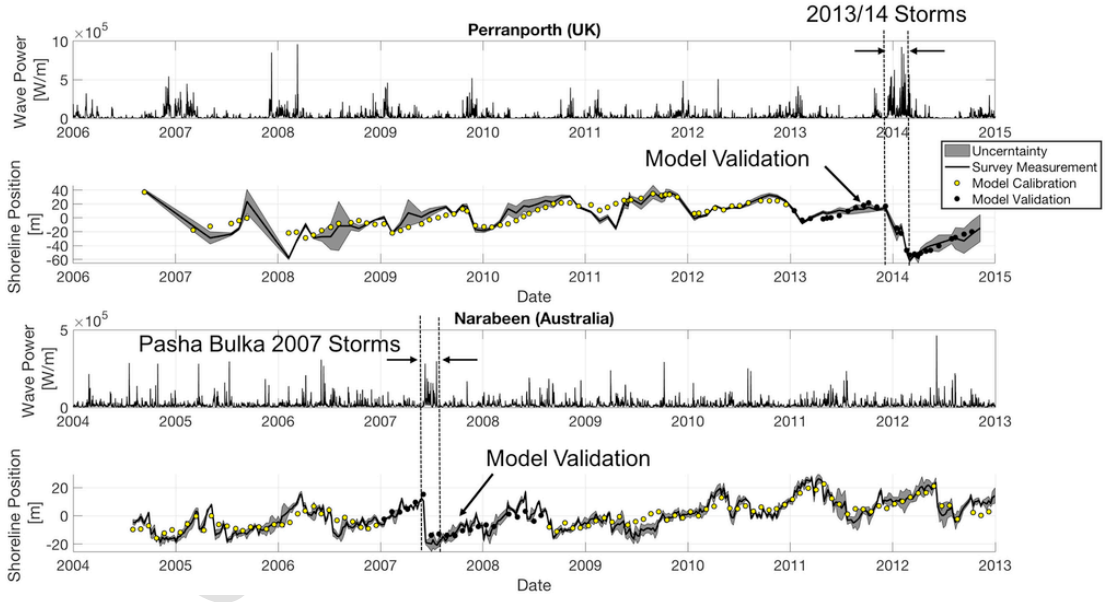

Fig. 3. The top two plots (a and b) show the 9-year wave power and associated shoreline displacements (mean high-tide contour) recorded at Perranporth. Also shown are the model calibration hindcasts and the unseen storm-validation hindcasts for the 2013/14 storms. The lower two plots are the equivalent series for Narrabeen (c and d). Notice that the Pasha Bulker June 2007 storm series has been used for the unseen model validation.

times series of both P and Ω. This is done by building multiple, annual time-series of P and Ω on a month-by-month basis, by selecting a random month long segments from a randomised pool of data containing only data from an equivalent month. The order of the months is shuffled randomly each time a simulation is made. The shuffling is done carefully, preserving the chronology of wave sequences within each month long record. Data are selected from the pool from a randomly selected starting location in order to produce unique records. This methodology preserves the seasonality, storm sequencing and joint probability of wave parameters. The size of the wave data pool for Perranporth and Narrabeen examples were 63 years and 36 respectively. The impact of the size of the data pool on predictions is examined later in this section.

In order for the test to be rigorous, the data pool used to generate the synthetic time-series must exclude the prediction period, even if the data are in fact known (i.e. hindcast). The data pool must also be consistent with the wave data used to calibrate and validate the model (same source or statistically similar).

A fundamental assumption underlying this method of synthetic wave generation is that future waves will be consistent with past wave conditions. Future modifications of the wave climate, due to climate change for example, are not included in these tests; a reasonable assumption for an annual time-scale of the predictions presented here. It is assumed that the wave data 2ϕ -days prior to the prediction date (t_0) is known (equivalent to the maximum width of filter function window (equation (3)), in order to evaluate the appropriate antecedent conditions, (Fig. 4). Each of the new synthetic time-series are concatenated on the end of these 2ϕ -days of observed data (Fig. 4). It is the combination of the known antecedent conditions and unknown future wave conditions which will determine the nature of the prediction. In fact, the seasonality in the synthetic series appears at first sight to be greater than in the 2ϕ -days of antecedent waves. This is because there are more extremes represented in the 10^3 simulations compared to the two antecedent years.

Fig. 5 shows an example of the resulting 10^3 Monte Carlo shoreline predictions corresponding to the synthetic forcing series. Notice that these simulations were started on the 1st October 2013, just prior to the extreme storms at Perranporth. Thus, the distribution shows an initial tendency for erosion (negative mean displacements), with recovery beginning in April and returning to near zero mean displacement by the end of the year. Notice also the spread in shoreline predictions for each month of the year, a distribution that will be characterised by the Generalised Extreme Value (GEV) analysis detailed in the next section.

3.4. Generalised extreme value (GEV) analysis

Here we extract from the shoreline prediction matrix the independent annual maximum values at regular time-steps. The analysis is done twice, once for erosion and once for accretion. The convention for accretion used here is a positive displacement, so extracting monthly maxima is straight forward. However, when repeating the process to compute the erosional values (which have a negative displacement), one must extract the maximum of the negative shoreline prediction matrix. Care is taken to use only unique shoreline series as the random generation method for the forcing series used here can potentially produce identical forcing and therefore replica shorelines. Typically, monthly intervals are used here, although this window duration can easily be varied. These monthly extremes from each of 10^3 simulations are plotted as histogram and a GEV probability distribution function (PDF) is fitted to the data. The GEV analysis used here focusses on accurately fitting the tails (extremes) of the distribution (rather than the peaks) and allows the data to instruct which of three distribution options is most appropriate to the observations (Kotz and Nadarajah, 2000). These options are controlled by a shape function k which dictates the decay structure at the limits of the distribution. Here an exponential decay is selected for $k = 0$ (e.g., normal, Gumbel (1958),), a polynomial for $k > 0$ (e.g. stu-

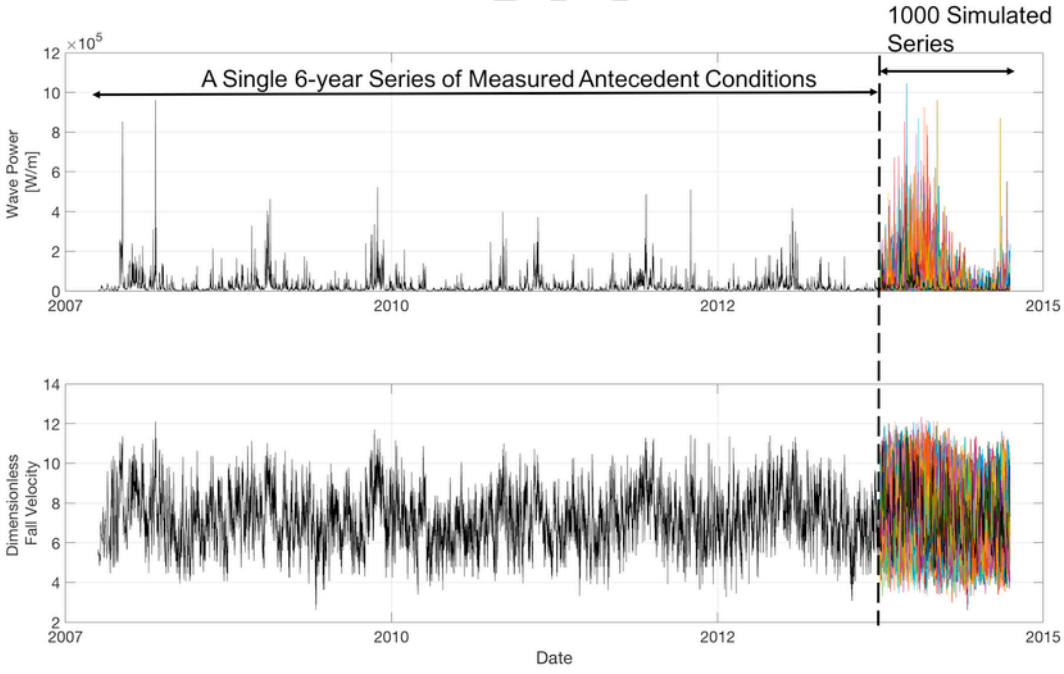

Fig. 4. An example of the synthetic forcing time-series (wave power [top] and dimensionless fall velocity [bottom]) used to drive the shoreline forecast. This is an annual forecast starting on the 1st October 2013 (dotted vertical line). Noticed that each record starts with 6-years of observed antecedent measurements to which 1000 different, year-long, synthetic series are appended.

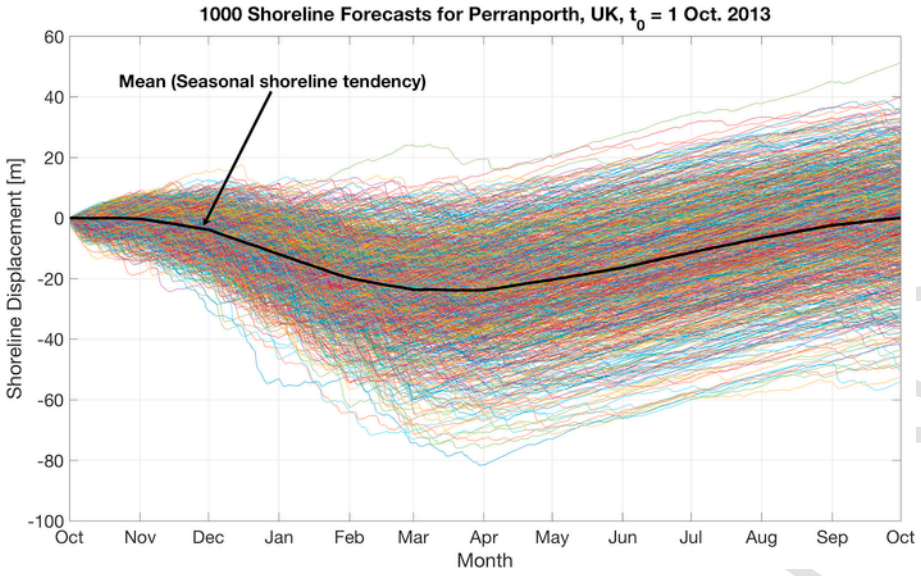

Fig. 5. This figure shows the 1000 resulting shoreline estimates generated from applying the forcing series in Fig. 4 to the ShoreFor model. The ensemble-mean tendency is shown by the solid black line, illustrating the seasonal trend in shoreline erosion and accretion.

dent's t-test, Fisher and Tippett (1928),), or $k < 0$ if the extreme is finite (e.g. Weibull (1951),). The form of the extreme value distribution PDF is:

$$y = f\,(x|k,\mu,\sigma) = exp\left[-exp\left\{-\left(\frac{x-\mu}{\sigma}\right)\right\}\right] \quad \text{for k} = 0 \quad ($$

or

$$y = f\,(x|k,\mu,\sigma) = exp\left\{-\left[1+k\left(\frac{x-\mu}{\sigma}\right)\right]^{-1/k}\right\} \quad \text{for k} \neq$$

Here μ is the location parameter, σ is the scale parameter and k is the shape parameter. The best fit of the GEV is obtained using the maximum likelihood method. For the specific case where the shape parameter $k < 0$ and the Weibull distribution is recovered (Coles, 2001), x (the shoreline displacement in this case) reaches an asymptotic limit as the return period ?∞, given by:

$$x_{max} = \mu - \sigma/k \quad (6)$$

This special case ($k < 0$) is worthy of mention here as it is pertinent to all the shoreline predictions and potentially relates the negative feedback in both erosion and accretion processes.

This methodology defines three erosion/accretion bands using a return level extrapolation on the GEV distribution, which has been fitted to the modelled shoreline data. Here we characterise the intensity of the cross-shore shoreline displacements with a colour-coded traffic light system. These three bands are normal (green), high (amber) and extreme (red) and described in detail below:

1) Normal (green): This band includes predictions which typify annual shoreline displacements with return periods of <10 years.
2) High (amber): These are predicted shoreline displacements with return periods in the range 10–100 years.
3) Extreme (red): This band defines extreme *events* with probabilities outside of the high band but encompassing the extremes of the predictions (x_{max}, equation (6))

The erosion and accretion bands are separated by the mean (central tendency) of the shoreline predictions, which calculated independently of the GEV analysis.

Fig. 6 shows a typical GEV analysis of accretion events for January 2014 from a prediction starting on 1 October 2013. The plot shows a comparison between the shoreline predictions and GEV PDFs [top left] and Q-Q plots [top right] of quantiles of the shoreline predictions and GEV model which should follow the straight line comparison if the model is to be deemed appropriate (Coles, 2001). Also shown are probability plots [bottom left] and the return level plot [bottom right] from which the traffic light bands are extracted. It can be observed from Fig. 6 that there is good linear agreement in the Q-Q and probability plots and the return value analysis is convex on this log-linear scale, indicating that the data are best fitted by a Weibull distribution ($k < 0$), with an upper asymptote for accretion of 18.8 m in this example (Coles, 2001).

A similar erosional example is shown in Fig. 7 for Perranporth. This prediction is for September 2014 from a simulation also starting on 1 October 2013. This analysis is based on the negative of the shoreline prediction matrix, but shows very similar results to the accretion example (Fig. 6). Again the shoreline predictions are best characterised by a Weibull distribution with an upper asymptote at −73.8 m.

3.5. Sensitivity of model predictions to the duration of the wave pool

It is unclear what impact the duration of the wave pool might have on the shoreline predictions. To gain further insight into this effect a sensitivity analysis was conducted by selecting a different number of randomly selected years from the Perranporth wave observations. These were then used to generate the 10^3 synthetic wave records and force the shoreline model. The number of years of wave data in the wave pool was varied between 10 and 60, and the subsequent impact

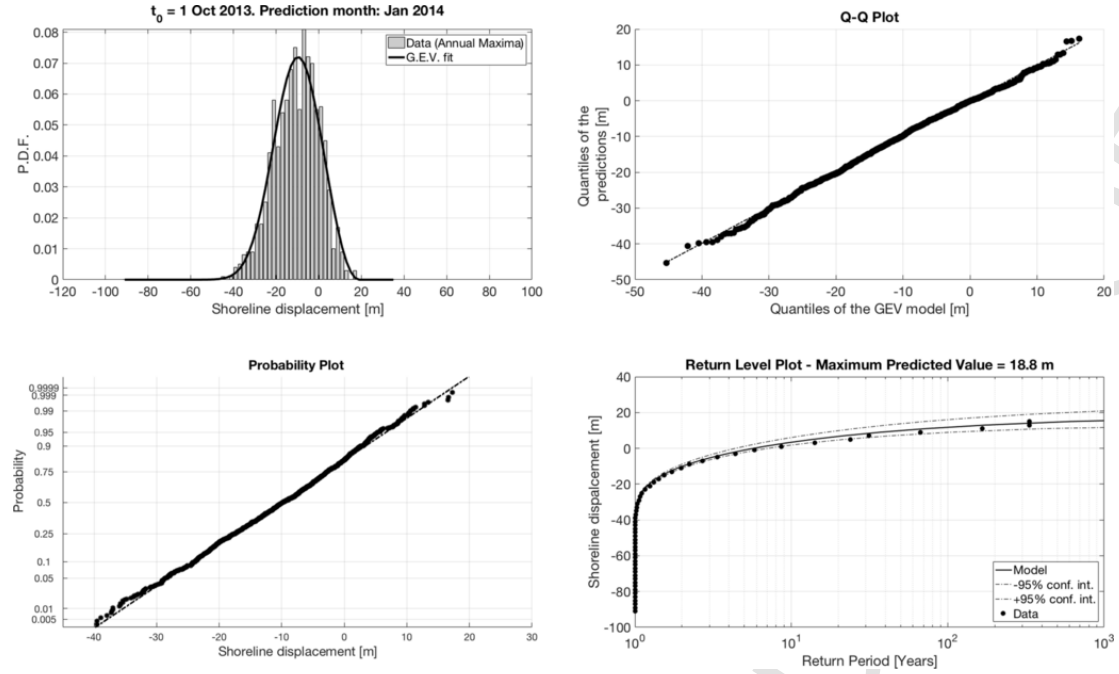

Fig. 6. Summary of GEV extrapolation of shoreline predictions of accretion for Perranporth, January 2014, 3.5 months ahead of the prediction start date. [Top left] Probability distribution of forecasted annual maximum accretion for January 2014, with fitted GEV distribution. [Top right] Q-Q plot comparing quantiles of the GEV fit with the shoreline predictions with a straight line comparison for assessing the model quality. [Bottom left] Probability plot for GEV fit and modelled shoreline maxima, with straight line comparison. [Bottom right] Return value extrapolation with 95% confidence intervals.

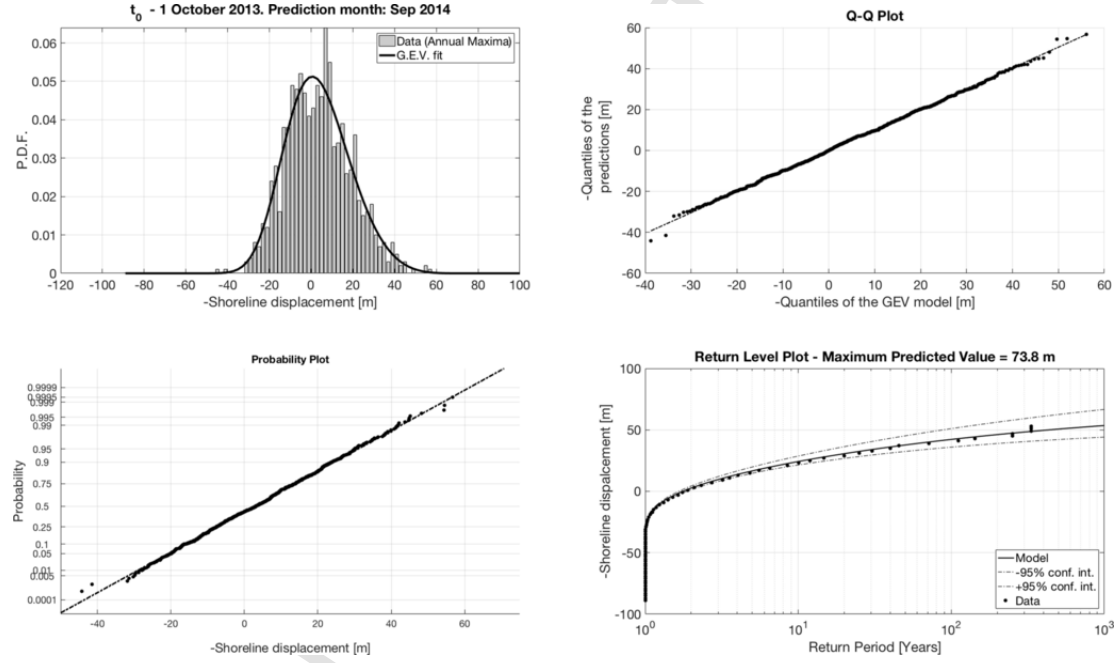

Fig. 7. Summary of GEV extrapolation of shoreline predictions of erosion for Perranporth, January 2014, 11.5 months ahead of the prediction start date. [Top left] Probability distribution of forecasted annual maximum erosion for September 2014, with fitted GEV distribution. [Top right] Q-Q plot comparing quantiles GEV fit with the shoreline predictions with a straight line comparison for assessing the model quality. [Bottom left] Probability plot for GEV fit and modelled shoreline maxima, with straight line comparison. [Bottom right] Return value extrapolation with 95% confidence intervals. Note that this analysis was conducted on the negative of the shoreline estimates, so maximum erosion is positive in these plots.

on the GEV fit parameters (k, σ and μ) and the 10, 50, 100 year return and maximum shoreline displacement values (x_{10}, x_{50}, x_{100} and $x_{\max}$) was assessed. The results of this analysis are summarised in Fig. 8. Inspection of Fig. 8 shows that the GEV fit values which determine the return values are more variable for wave pool sizes less than about 25 years, after which they remain roughly similar, with little further increase in stability up to 60 years. The same is true of the estimates of x_{10}, x_{50} and x_{100}. It is also worthy of note that whilst of x_{10},

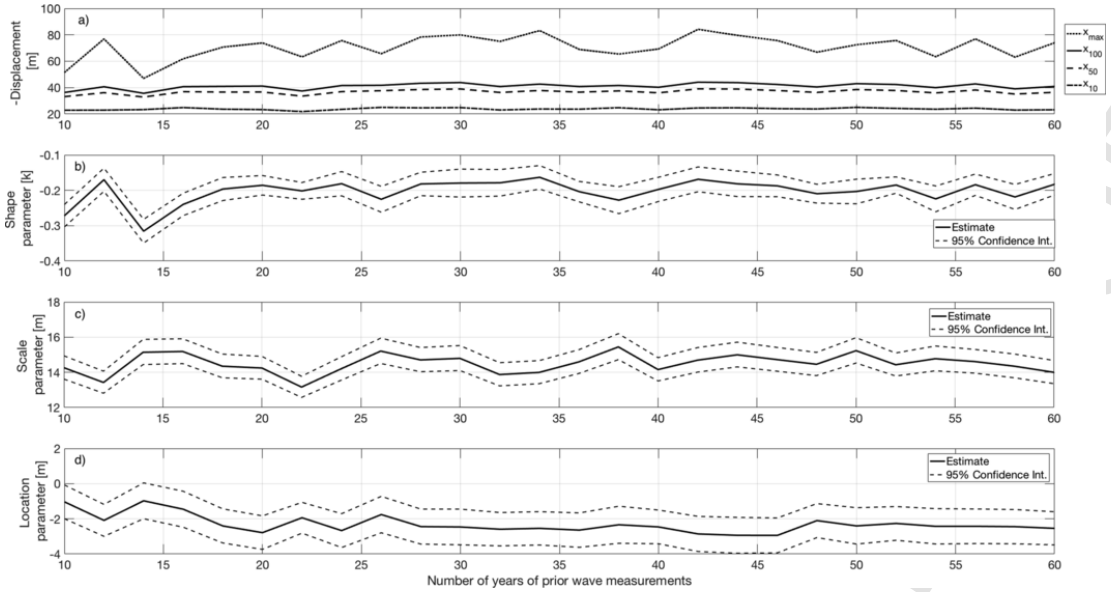

Fig. 8. Sensitivity analysis on the duration of the wave pool used to generate the synthetic wave time-series. Here the number of years of data used to simulate the 1000 shoreline estimates have been randomly selected from the original wave pool. This simulation was run for Perranporth with predictions in September 2014, with t_0 = 1 October 2013. [a] Estimation of the maximum shoreline erosion, 100, 50 and 10-year return erosion levels. [b] GEV shape parameter with 95% confidence intervals. [c] GEV scale parameter with 95% confidence intervals. [d] GEV location parameter with 95% confidence intervals.

x_{50} and x_{100} remain quite stable statistics (±2 m) for pool sizes in excess of 25 years, the most extreme statistic x_{max}, remains rather noisy and unreliable. Based on this analysis the authors suggest that the wave pool size should exceed 25-years in order to achieve consistent forecast classifications, although a firm conclusion on this point will probably require experimentation at additional sites.

3.6. Sensitivity of model predictions to the number of synthetic wave time-series

In this section the sensitivity of the predictions and GEV fit parameters to the number of synthetic time series used to force the shoreline model. Here we vary the number of simulation from 20 to 1000, whilst monitoring the convergence and uncertainty in the GEV parameters (k, σ and μ) and the impact on the shoreline estimates (x_{10}, x_{50}, x_{100} and x_{max}). The results of this analysis are summarised in Fig. 9. There is substantial variability and uncertainty in all parameters for less than 800 simulations, after which all parameters converge. An interesting point to note is that the estimates using 1000 simulations are more conservative (higher) than those using an equal number of simulations to the number of years in the wave pool (vertical dotted line in Fig. 9). This is because a higher number of simulations increases the possibility of bringing together all of the most energetic months into a single year. Thus, the impact of increasing the number of simu-

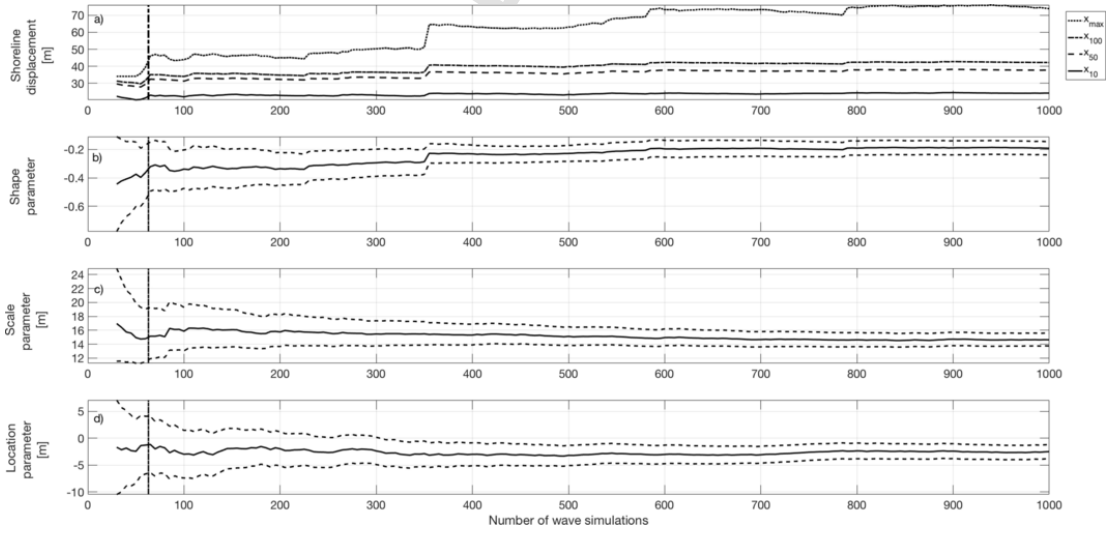

Fig. 9. Sensitivity analysis on the number of years of synthetic wave data used to generate shoreline predictions. This simulation was run for Perranporth with predictions in September 2014, with t_0 = 1 October 2013. [a] Estimation of the maximum shoreline erosion, 100, 50 and 10-year return erosion levels. [b] GEV shape parameter with 95% confidence intervals. [c] GEV scale parameter with 95% confidence intervals. [d] GEV location parameter with 95% confidence intervals. The vertical dotted line represents the number of years of data in the wave pool.

lations to >800 is to increase the stability and uncertainty of the estimate and produce more conservative estimates of erosion and accretion. Based on this analysis all future predictions are based on 10^3 synthetic wave records.

4. Results

4.1. Perranporth, UK

Fig. 10 shows both the predicted and measured shoreline impact and subsequent recovery of the 2013/14 winter storms at Perranporth. In order to capture a complete season of recovery-erosion-recovery, predictions start 7-months prior to the main storm impacts on the 1st May 2013 during the beach recovery phase and proceeds with start times (t_0) incrementing in two-month intervals through the storm and up to the start of the post-storm recovery. In doing so we are able to answer two key coastal management questions, namely: Can we predict the likely impact of the next extreme storm sequence? And, can we predict beach recovery after the impacts of an extreme storm sequence?

Fig. 10a shows the shoreline predictions during the recovery period, prior to the main storm. A narrow range of potential shoreline projections are predicted over the coming six-months. It is not until the onset of the winter storms, when there is a tendency for erosion that the predicted range in shoreline responses widens significantly. Inspection of the measured data in this plot shows that shoreline recovery in this example (Fig. 10) is slow initially, remaining in the lower-amber range during the period leading up to the storms, but reaching the low-normal (green) range by December 2013.

Pre-storm shoreline positions were at the shoreward-extreme of the normal range prior to the storms (i.e. somewhat eroded for the time of year). In all cases the data are effectively captured within the prediction band and the range of the predictions is not so excessive as to be of limited value. This example (Fig. 10a) shows that for this seasonally dominated site, shoreline recovery is indeed predictable.

The classification of the observed 2013/14 storm impact (see arrow in Fig. 10a), starting 11 months before the maximum observed erosion is extreme (red). This rating has a return period of >100 years. This extreme (red) classification of the storm persists throughout the pre-storm period (Fig. 10a–c). This classification is consistent with the observation that the 2013/14 storms were the largest sequence of storm waves observed during the prior 60 years of wave of wave measurements.

The post extreme-storm recovery is predicted after the 2013-14 storms, starting t_0 = 1st March 2014 in Fig. 10f. It can be seen in this second recovery example, that once again, the prediction is tight and accurate. Unlike the pre-storm recovery (Fig. 10a), the post recovery is much more rapid, proceeding in the upper-amber range. This was somewhat unexpected as the offshore survey data (not included here) showed that the eroded beach sand had been moved to an offshore bar, located 1 km offshore of the high-tide shoreline position. This extreme translation of sand does not seem to have stunted beach recovery at all. Notice however, that there is quite a bit of uncertainty in the measurements, represented by the error bars in the data during this recovery phase as the beach gets more 3-dimensional in the longshore direction as the sand moves from the offshore sandbar towards beach. Again, Fig. 10f supports the notion that beach recovery is indeed predictable at this site. Notice also that the methodology used here may predict different outcomes for the same month in different years, due to importance and potentially different antecedent hydrodynamic conditions.

4.2. Narrabeen, Australia

Perhaps a more challenging test for this methodology is application to a distinctly storm dominated wave climate, with a weaker seasonal signal, where shoreline responses are more rapid. The Narrabeen dataset provides the opportunity to do this. Like the previous Perranporth example, Fig. 11a starts during the natural recovery-phase on the 1st October 2006, prior to the Pasha Bulker storm sequence. An identical methodology to that used in the previous example at Perranporth has been applied here to an extreme storm sequence at Narrabeen.

It can be seen that the prediction for Narrabeen still provides a useful estimate of shoreline recovery, even in this storm dominated environment (Fig. 11a). Comparison with the measured data shows that unlike Perranporth the recovery at Narrabeen prior to the storm is high, lying entirely within the upper end of the normal range

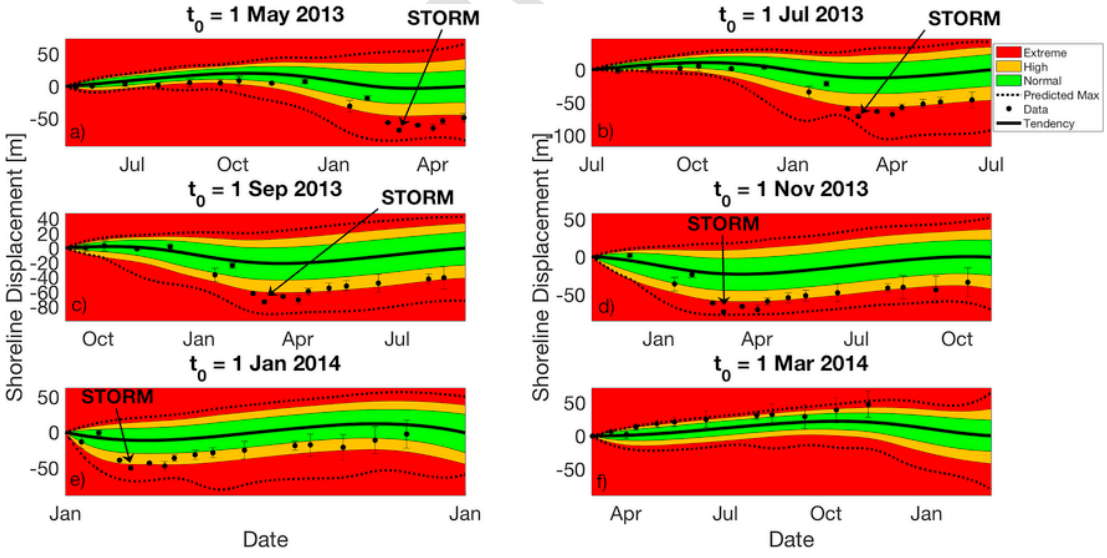

Fig. 10. Six forecasts of shoreline displacements for Perranporth Beach, UK (seasonally dominated system), starting during the pre-storm recovery period in May and progressing in 2-mothly intervals until the post-storm recovery period in March 2014. The arrow indicates the maximum shoreline recession due to the storm in each case.

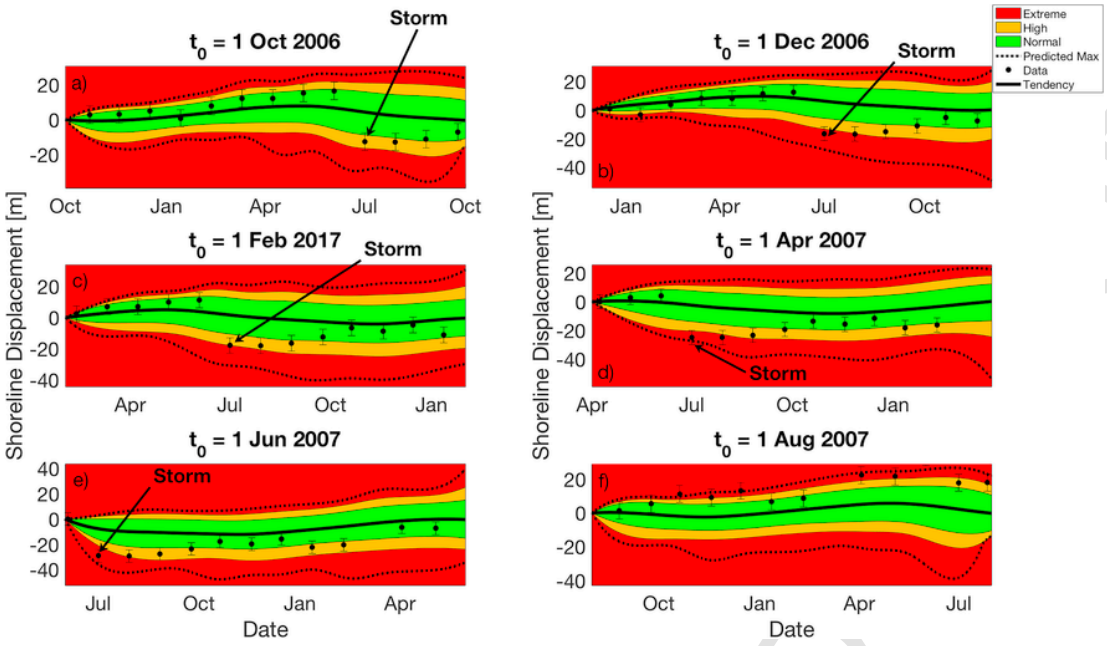

Fig. 11. Forecasted shoreline response for Narrabeen, Australia (storm dominated system). Forecasts start with t_0 at the pre-storm recovery phase in October 2006 and progress at two-monthly intervals through the main storm sequence in June 2007 and to the post-storm recovery starting in August 2007.

(upper-green/amber boundary). This healthy recovery led to high levels of shoreline accretion prior to the inception of the Pasha Bulker storm sequence.

Notice also that the maximum storm erosion, indicated by the arrow, is in all of the pre-storm predictions (Fig. 11a–e), is not as extreme as Perranporth but consistently lies on the erosional amber-red boundary, indicating that shoreline displacement due to the Pasha Bulker storm sequence, like the Perranporth example, has an event probability of ≈1/100. Interestingly, shoreline positions and beach volumes along the New South Wales coastline were not observed to have eroded excessively and certainly would have not been at 1/100-year low after this storm sequence. It is important to acknowledge here that this methodology is characterising shoreline displacement, rather than absolute shoreline position. Whilst these two measures are similar, large erosion events should correlate with an eroded shoreline, they are not the same thing. In this example, the pre-storm shoreline was quite strongly pro-graded, thus, in spite of considerable storm erosion, the post-storm shoreline was not excessively eroded.

Shoreline recovery after the Pasha Bulker storm is predicted in Fig. 11f. Like the post storm Perranporth example, beach recovery is well predicted at Narrabeen and is rapid, skirting both the amber (high) red (extreme) intersection.

5. Concluding remarks and future work

A new methodology for predicting shoreline displacement has been detailed in this contribution. The methodology includes: generating multiple forcing time-series based on measured or modelled wave data, the implementation of an established shoreline model (Davidson et al., 2013) to drive a Monte Carlo prediction of shoreline behaviour and extrapolating these shoreline responses with a generalised extreme value (GEV) analysis. Results presented here indicate that it is indeed possible, at least on these exposed, swash-aligned sites, to provide genuine prediction of the limits of:

a) Shoreline recession due to the impact of a storm sequence.
b) Shoreline recovery after the passage of an extreme storm erosion events.

The methodology provides a probabilistic prediction (PDF) of shoreline displacements, up to a year in advance of the prediction start date and a simplistic 'traffic light' classification classifying erosion events as normal, high or extreme. Shoreline predictions are classified as normal (likely to be observed once in a decade), high (10 years < return periods <100 years) and extreme (return periods >100 years).

Although the methodology has been tested on time-series of shoreline displacement, it could easily be transferred to the prediction of other definitions of the shoreline position or indeed intertidal beach volumes. Here we use an established shoreline model, ShoreFor (Davidson et al., 2013), but acknowledge that the same methodology could be equally well implemented with other fast and robust models of this genre. The present model is restricted to coasts dominated by cross-shore sediment transport, but other modelling approaches could be combined with this general prediction methodology, including one-line models, in order to overcome these limitations.

In both applications presented here the models showed highly skilful hindcasts. This is an essential pre-requisite of this approach. Poor model hindcasts are likely to lead to unreliable predictions. Here we recommend the model-data calibration coefficients (r) (comparisons between observations and model results) exceed 0.8 for accurate predictions. Weaker correlations could lead to under-predict the magnitude of the shoreline response.

This contribution used measured shoreline data to calibrate the shoreline model. However, the availability of shoreline data is not necessarily a limit to application of this particular model. Splinter et al. (2014)., showed that ShoreFor model free parameters can be estimated using easily available environmental parameters including wave climate and sediment properties.

A provisional sensitivity analysis shows that the minimum size of the pool of wave data required to produce accurate and consistent predictions of shoreline response is approximately 25-years, although it is recommended that all the available data are used. In the simulations used here we have implemented predictions with both modelled (Perranporth) and a mixture of measured/modelled (Narrabeen) wave data, both provided good estimates of shoreline behaviour. Since the use of commonly available modelled wave data seems to provide robust shoreline predictions, the application of this methodology could potentially be quite widely used for the prediction of extreme shoreline erosion and subsequent beach recovery.

Recent studies indicate that climatic indices can be skilfully predicted a year in advance (Dunstone et al,. 2016). The fact that climate indexes (e.g. NAO and ENSO) have been linked to storminess and shoreline change (e.g. Robinet et al., 2016), indicates that it may be possible to make more accurate predictions for the forthcoming year and perhaps beyond, if the synthetic waves used to force the shoreline predictions were based only on past wave data with climate indexes similar to those projected for the prediction period.

Uncited references

Davidson et al., 2007b; Dunstone et al., 2016; Frazer et al., 2009; French et al., 2016; Liu and Burcharth, 1999.

Acknowledgements

A special thanks to Gerd Masselink, Paul Russel, Tim Scott, Tim Poate, Martin Austin, Kit Stokes, Peter Ganderton and all others who contributed to the Perranporth data set included in this paper. This research was funded by the Australian Research Council Discovery Grant DP150101339. Mark Davidson would like to extend a special thanks to Water Research Laboratory, School of Civil and Environmental Engineering, UNSW Sydney for additional funding and hosting his visits to work with the Australian team and to all of the staff at the Water Resources Laboratory for making this such a pleasant and productive sabbatical.

References

Ashton, A.D., Murray, A.B., 2006. High-angle wave instability and emergent shoreline shapes:1 Modeling of sand waves, flying spits, and capes. J. Geophys. Res. Earth Surf. (2003–2012) 111 (F4).

Ashton, A.D., Murray, A.B., Arnoult, O., 2001. Formation of coastline features by large-scale instabilities induced by high-angle waves. Nature 414 (6861), 296–300.

Baart, F., van Ormondt, M., de Vries, J.S.M.van Thiel, van Koningsveld, M., 2016. Morphological impact of a storm can be predicted three days ahead. Comput. Geosci. 90 (B), 17–23.

Borgman, L.E., Scheffner, N.W., 1991. Simulation of Time Sequences of Wave Height, Period, and Direction. Technical Report DRP-91–92,54. US Army Corps of Engineers, Washington.

Callaghan, D.P., Nielsen, P., Short, A.D., Ranasinghe, R., 2008. Statistical simulation of wave climate and extreme beach erosion. Coast. Eng. 55 (5), 375–390.

Callaghan, D.P., Ranasinghe, R., Roelvink, D., 2013. Probabilistic estimation of storm erosion using analytical, semi-empirical, and process based storm erosion models. Coast. Eng. 82, 64–75, 2013.

Cloke, H.L., Pappenberger, F., 2009. Ensemble flood forecasting: a review. J. Hydrology 375 (3–4), 613–626.

Coles, S., 2001. An Introduction to Statistical Modelling of Extreme Values. 216pp, Springer, London.

Davidson, M.A., Turner, I.L., 2009. A behavioural template beach profile model for predicting seasonal to inter-annual shoreline evolution. J. Geophys. Res. 114, 1–21.

Davidson, M.A., Huntley, D.A., Holman, R.A., George, K., 1997. The evaluation of large-scale (km) intertidal beach morphology on a macrotidal beach using video images. In: Proceedings Coastal Dynamics '97. ASCE, pp. 385–394.

Davidson, M.A., Van Koningsveld, M., de Kruif, A., Rawson, J., Holman, R., Lamberti, A., Medina, R., Kroon, A., Aarninkhof, S., 2007. The CoastView project: developing video- derived coastal state indicators in support of coastal zone management. Coast. Eng. 54 (6–7), , 463–475. https://doi.org/10.1016/j.coastaleng.2007.01.007.

Davidson, M.A., Lewis, R.P., Turner, I.L., 2010. Forecasting seasonal to multi-year shoreline change. Coast. Eng. 57, 620–629. https://doi.org/10.1016/j.coastaleng.2010.02.001.

Davidson, M.A., Splinter, K.D., Turner, I.L., 2013. A simple equilibrium model for predicting shoreline change. Coast. Eng. 73, 191–202, Available at: http://www.sciencedirect.com/science/article/pii/S0378383912001676.

Day, G.N., 1985. Extended Streamflow forecasting using NWSRFS. J. Water Resour. Plan. Manag. 111 (2).

Dodet, G., Bertin, X., Taborda, R., 2010. Wave climate variability in the North-East Atlantic Ocean over the last six decades. Ocean. Model. 31, 120–131.

Dunstone, N., Smith, D., Scaife, A., Hermanson, L., Eade, R., Robinson, N., Andrews, M., Knight, J., 2016. Skilful predictions of the winter North Atlantic Oscillation one year ahead. Nat. Geosci. 9, 809–814. https://doi.org/10.1038/ngeo2824.

Farris, A.S., List, J.H., 2007. Shoreline as a proxy for subaerial beach volume change. J. Coast. Res. 23 (3), 740–748.

Fisher, R.A., Tippett, L.H.C., 1928. Limiting forms of the frequency distribution of the largest and smallest member of a sample. In: Proc. Cambridge Philosophical Society 24. pp. 180–190.

Frazer, N.L., Genz, A.S., Fletcher, C.H., 2009. Toward parsimony in shoreline change prediction (I): basis function methods. J. Coast. Res. 25 (2), 366–379.

Gourlay, M.R., 1968. Beach and Dune Erosion Tests. Rep. M935/M936. Delft Hydraulics Laboratory, Delft, Netherlands.

Gumbel, E.J., 1958. Statistics of Extremes. Columbia University Press, New York.

Hanson, H., 1989. GENESIS: a generalized shoreline change model. J. Coast. Res. 5 (1), 1–27.

Hanson, H., Kraus, N., 1989. Generalized Model for Simulating Shoreline Change, Report 1, Technical Reference, Tech. Rep., U. S. Army Engineer Waterways Experiment Station; Coastal Engineering Research Center (U. S.). United States. Army. Corps of Engineers.

Harley, M.D., Turner, I.L., Short, A.D., Ranasinghe, R., 2010. Interannual variability and controls of the Sydney wave climate. Int. J. Climatol. 1335, 1322–1335.

Harley, M.D., Turner, I.L., Short, A.D., Ranasinghe, R., 2011. Assessment and integration of conventional, RTK-GPS and image-derived beach survey methods for daily to decadal coastal monitoring. Coast. Eng. 58 (2), 194–205.

Harley, M.D., Turner, I.L., Splinter, K.D., Phillips, M.S., Simmons, J.A., 2016. Beach response to australian east coast lows: a comparison between the 2007 and 2015 events, narrabeen-collaroy beach. J. Coast. Res. SI 75, 388–392.

Kotz, S., Nadarajah, S., 2000. Extreme Value Distributions: Theory and Applications. Imperial College Press, London.

Kroon, A., Davidson, M.A., Aarninkhof, S.G.J., Archetti, R., Armaroli, C., Gonzalez, M., Medri, S., Osorio, A., Aagaard, T., Holman, R.A., Spanhoff, R., 2007. Application of remote sensing video systems to coastline management problems. Coast. Eng. 54 (6–7), 493–505. https://doi.org/10.1016/j.coastaleng.2007.01.004.

Larson, M., Kraus, N.C., 1989. SBEACH. Numerical Model for Simulating Storm Induced Beach Change; Report 1. Empirical Foundation and Model, Development, 0749– 9477.

Lord, D., Kulmar, M., 2000. The 1974 storms revisited: 25-years experience in ocean wave measurement along the south-east Australian coast. In: Proceedings, International Coastal Engineering Conference, Sydney. pp. 559–572.

Masselink, G., Short, A.D., 1993. The effect of tidal range on intertidal beach morphology: a conceptual model. J. Coast. Res. 9, 785–800.

Masselink, G., Austin, M., Scott, T., Poate, T., Russell, P., 2014. Role of wave forcing, storms and NAI in outer bar dynamics on a high energy, macro-tidal beach. Geomorphology 226, 76–93.

Masselink, G., Scott, T., Poate, T., Russell, P., Davidson, M., Conley, D., 2014. The Extreme 2013/2014 Winter Storms: Hydrodynamic Forcing and Coastal Response along the Southwest Coast of England, Earth Surface Processes and Landformshttps://doi.org/10.1002/esp. 3836.

Murray, A.B., 2007. Reducing model complexity for explanation and prediction. Geomorphology 90 (3), 178–191.

Prodger, S., Russell, P.E., Davidson, M.A., Scott, T., 2015. Understanding and predicting the temporal variability of sediment grain size characteristics on high-energy beaches. Mar. Geol. 376 (1 June 2016), 109–117.

Ranasinghe, R., Mcloughlin, R., Short, A.D., Symonds, G., 2004. The Southern Oscillation Index, wave climate, and beach rotation. Mar. Geol. 204, 2–7.

Reeve, D.E., Pedrozo-Acuña, A., Spivack, M., 2014. Beach memory and ensemble prediction of shoreline evolution near a groyne. Coast. Eng. 86 (April 2014), 77–87.

Robinet, A., Castelle, B., Idier, D., Le Cozannet, G., Deque, M., Charles, E., 2016. Statistical modelling of Interannual shoreline change driven by North Atlantic climate variability spanning 2000-2014 in the Bay of Biscay. Geo-Mar. Lett. https://doi.org/10.1007/s00367-016-0460-8.

Ruggiero, P., List, J., Hanes, D., Eshleman, J., 2006. Probabilistic shoreline change modelling. In: Proc. 30th International Conference on Coastal Engineering, September 2006, San Diego, CA.

Short, A.D., Trenaman, N.L., 1992. Wave climate of the Sydney region, an energetic and highly variable ocean wave regime. Aust. J. Mar. Freshw. Res. 43, 765–791.

Splinter, K.D., Turner, I.L., Davidson, M.A., Barnard, P., Castelle, B., Oltman-Shay, J., 2014. A generalized equilibrium model for predicting daily to inter-annual shoreline response. J. Geophys. Res. Earth Surf. 1936–1958.

Thomas, T., Phillips, M.R., Williams, A.T., Jenkins, R.E., 2012. Medium-scale behaviour of adjacent embayed beaches: influence of low energy external forcing. Appl. Geogr. 32, 265–280.

Turki, I., Medina, R., Gonzalez, M., Coco, G., 2013. Natural variability of shoreline position: observations at three pocket beaches. Mar. Geol. 338, 76–89. https://doi.org/10.1016/j.margeo.2012.10.007.

Turner, I.L., Harley, M.D., Short, A.D., Simmons, J.A., Bracs, M.A., Phillips, M.S., Splinter, K.D., 2016. A Multi-decade Dataset of Monthly Beach Profile Surveys and Inshore Wave Forcing at Narrabeen, Australia. Scientific Data 3, 160024https://doi.org/10.1038/sdata.2016.24.

Walstra, D.J.R., Reniers, A.J.H.M., Ranasinghe, R., Roelvink, J.A., Ruessink, B.G., 2012. On bar growth and decay during inter-annual net offshore migration. Coast. Eng. 60, 190–200. https://doi.org/10.1016/j.coastaleng.2011.10.002.

Walstra, D.J.R., Wesselman, D.A., van der Deijl, E.C., Ruessink, B.G., 2016. On the intersite variability in inter-annual nearshore sandbar cycles. J. Mar. Sci. Eng. 4 (1), 15. https://doi.org/10.3390/jmse4010015.

Weibull, W., 1951. A statistical distribution function of wide applicability. J. Appl. Mech. Trans. ASME 18 (3), 293–297.

Wright, L.D., Short, A.D., Green, M.O., 1985. Short-term changes in the morphodynamic states of beaches and surfzones: an empirical predictive model. Mar. Geol. 62, 339–364.

Yates, M.L., Guza, R.T., O'Reilly, W.C., 2009. Equilibrium shoreline response: observations and modeling. J. Geophys. Res. 114 (C09014)https://doi.org/10.1029/2009JC005359.

Yates, M.L., Guza, R.T., O'Reilly, W.C., Hansen, J.E., Barnard, P.L., 2011. Equilibrium shoreline response of a high wave energy beach. J. Geophys. Res. 116 (C04014)https://doi.org/10.1029/2010JC006681.